Dynamic Performance Comparison for Improved Vector and Scalar Controlled Asynchronous Motor Drives

Hadi Naghizadeh Ghishlagh [1], Hossein Nasiraghdam [1], Mohsen Ebadpour [2] (Corresponding Author)
[1] Department of Electrical Engineering, Ahar Branch, Islamic Azad University, Ahar, Iran
[2] Faculty of Electrical Engineering, University of West Bohemia (UWB), Pilsen, Czech Republic
Email: hadinaqiahar@gmail.com [1], hossein_nasiraghdam@yahoo.com [1], mohsenebadpour2@gmail.com [2]
Receive Date: 01 Jan 2024 Accept Date:12 April 2024

Abstract

This article presents comparative studies for dynamic performance evaluation of vector- and scalar-controlled asynchronous (induction) motor (ASM) drives based on improved control baselines. To compare the ASM drive responses, four control strategies including improved direct torque control (DTC), improved indirect field-oriented control (IFOC), feedback (FB) linearization, and scalar vectorized Volt per Hertz (VV/Hz) are considered with their enhanced versions based on the space vector pulse-width modulation (SVPWM) switching technique. The main objective of this work is to implement feasible dynamic computer functions of the ASM drive to assess its torque and speed responses over the variable low and high speeds for pure or hybrid electric vehicle traction drive applications using MATLAB/Simulink software. To validate the overall performance of the ASM drive, several case studies are developed to evaluate the transient behavior of the system from the starting stage to the steady state over the variable load conditions.

Keywords: Asynchronous motor (ASM), vector control, direct torque control (DTC), field-oriented control (FOC), scalar control, SVPWM technique, dynamic performance.

1. Introduction

The most common type of electric motors employed in industries are asynchronous motors (ASMs), mostly named induction motors, due to their robustness, reliability, and low manufacturing cost. The main challenge with an ASM is speed control requires relevant controllers, power converters, and sensors. Advancements in switching devices technology soon rectified this challenge with suitable power electronic converters [1-3]. In order to evaluate an ASM drive performance, the motor is vastly modeled in a reference frame that orients synchronously or with magnetic flux using appropriate control strategies with or without speed sensors [4], [5]. Owning to the enormous application of ASM drives in various industrial places, simulation and dynamic modeling of them have been significant to both academia and businesses. The merit of dynamic modeling is that it accelerates understanding of ASM performance in dynamic mode as well as steady-state operations [6].

Industries and electric vehicle (EV) companies frequently employ adjustable speed drives to link ASM actuators to the main power supply through a voltage source inverter (VSI). Several studies have been developed for VSI-fed three-phase ASM drives with different closed-loop control baselines for steady-state and dynamic operational modes. These approaches

include direct torque control (DTC) [7]; rotor field-oriented control (FOC) [8]; model predictive control (MPC) [9]; conventional or hybrid voltage per frequency (V/f) scalar control [10], [11]; and other vector control approaches to acquire optimal performance within user-defined demands [12-14]. Among the aforementioned approaches, MPC and DTC output variable switching frequency to gain optimum torque and flux requirements. However, the rotor flux FOC baseline uses various carrier-based pulse width modulation (PWM) switching techniques [15]. To control the output voltage of three-phase VSI and mitigate its harmonic distortion, different PWM control strategies have commonly been adopted in three-phase ASM drives. Several of those closed-loop PWM baselines utilize the space-vector PWM (SVPWM) technique to minimize switching losses with constant switching frequency owing to the higher using of DC link voltage in SVPWM [16].

To better distinguish the mentioned control strategies responses for ASM drives, the four most common control approaches including DTC, indirect FOC (IFOC), vectorized V/f (VV/Hz), and feedback (FB) linearization are dynamically modeled and their responses compared in this article. To improve the performance of the DTC and IFOC techniques, the SVPWM scheme is also used for their switching method. Furthermore, the VV/Hz control baseline is developed instead of conventional V/f control to improve the ASM drive speed and torque requirements as a simple control strategy. The main contribution of this study is to accurately illustrate the differences among the ASM drives' performances to give feasible authority for consumers to properly select their demanded drives. In section 2, the studied ASM drive systems and their dynamic models are described. Comparative case studies and simulation results are shown in section 3.

2. ASM Drive Systems

The general drive system of a three-phase VSI-fed ASM is illustrated in Fig. 1. From the figure, the main parts of an ASM drive system include a VSI, an ASM, a controller along with a switching scheme, and mechanical/electrical sensors for data acquisition. The dynamic model of a symmetrical three-phase ASM can be developed using basic mechanical and electrical equations of the motor vastly in the synchronous reference frame with d- and q-axis states [17] as follows

$$\frac{d\lambda_{qs}}{dt} = -r_s i_{qs} - \omega_s \lambda_{ds} + v_{qs} \quad (1)$$

$$\frac{d\lambda_{qs}}{dt} = -r_s i_{ds} + \omega_s \lambda_{ds} + v_{ds} \quad (2)$$

$$\frac{d\lambda_{qr}}{dt} = -r_r i_{qr} - \left(\omega_s - n_p \omega_r\right)\lambda_{dr} + v_{qr} \quad (3)$$

$$\frac{d\lambda_{dr}}{dt} = -r_r i_{dr} + \left(\omega_s - n_p \omega_r\right)\lambda_{qr} + v_{ds} \quad (4)$$

$$\frac{d\omega_r}{dt} = \frac{3}{2}\frac{n_p}{J}\left(\lambda_{ds} i_{qs} - \lambda_{qs} i_{ds}\right) - \frac{T_L}{J} \quad (5)$$

where v_s and v_r are stator and rotor voltages; i_s and i_r are stator and rotor currents; λ_s and λ_r are stator and rotor flux linkages; r_s and r_r are stator and rotor resistances referred to the stator; ω_s and ω_r are stator angular frequency and rotor electrical speed in (rad/sec); n_p is the number of pole pairs; J is the total motor and load moment of inertia; and T_L denotes load torque.

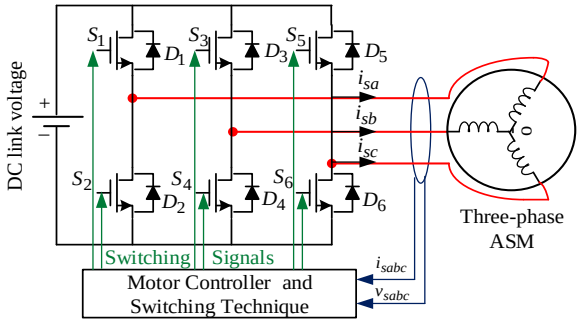

Fig. 1. Two-level VSI-fed three-phase ASM drive system.

2.1. Improved DTC-SVPWM

The developed DTC-SVPWM scheme of speed and torque control is derived from the conventional DTC scheme [7], which includes the desirable feature of employing the SVPWM switching scheme instead of the classic PWM algorithm. However, one of the main issues with the conventional DTC scheme is that it mostly contains hysteresis regulators for the flux and torque controls which lead to variable switching frequencies and high amounts of torque ripples. In this work, the implemented approach is improved to make the ASM drive with smooth operation with low torque ripples via using PID controllers instead of hysteresis regulators. Fig. 2 shows the overall block diagram of the improved DTC-SVPWM scheme.

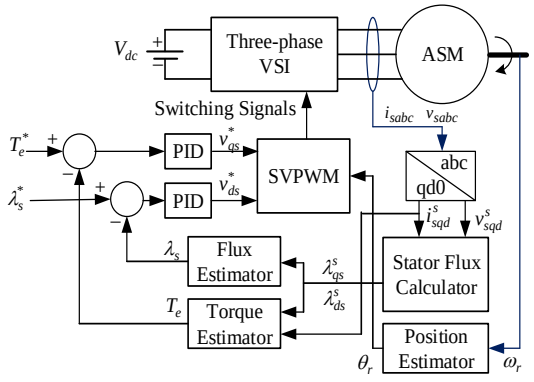

Fig. 2. Improved DTC-SVPWM controlled ASM drive system.

From Fig. 2, the electromagnetic torque (T_e) and stator linkage flux (λ_s) can be calculated as follows

$$T_e = \frac{3}{2} n_p \left(\lambda_{ds} i_{qs} - \lambda_{qs} i_{ds}\right) \quad (6)$$

$$\lambda_s = \sqrt{(\lambda_{qs}^2 + \lambda_{ds}^2)} \quad (7)$$

The calculated T_e and λ_s are compared with their reference values and the corresponding errors after regulating with the PID controllers, are utilized to determine the reference voltages in d-q terms. Consequently, the SVPWM module generates the proper switching signals for the VSI through the controlled reference voltages and using estimated/measured ASM rotor position information.

2.2. Improved IFOC-SVPWM

The IFOC baseline as an indirect vector controller originated from the dynamic equations of the ASM in the synchronous reference frame [8]. Similar to the conventional DTC-PWM approach with hysteresis regulators, IFOC-PWM also contains high torque ripple which leads to more acoustic noise during dynamic performance. To solve this issue, the IFOC-SVPWM with a classic PID speed regulator is developed as shown in Fig. 3. From Fig. 3, the main function is the calculation of stator voltage references (i.e. v_{qs}^{s*} and v_{ds}^{s*}) in the synchronously rotating reference frame (indicated by variables with superscript s) as follows

$$v_{qs}^{s*} = \sigma\left\{-n_p \omega_r i_{ds}^s - \frac{L_m}{\tau_r} i_{ds}^s \frac{(i_{qs}^s \lambda_{ds}^s - i_{ds}^s \lambda_{qr}^s)}{(\lambda_s^s)^2} - \frac{\lambda_{dr}^s \omega_r^*}{\lambda_s^s} + \frac{\lambda_{qr}^s \lambda_s^*}{\lambda_r^s}\right\} - \frac{L_m n_p \omega_r \lambda_{dr}^s}{L_r} \quad (8)$$

$$v_{ds}^{s*} = \sigma\left\{-n_p\omega_r i_{qs}^s - \frac{L_m}{\tau_r} i_{qs}^s \frac{(i_{qs}^s\lambda_{dr}^s - i_{ds}^s\lambda_{qr}^s)}{(\lambda_r^s)^2} - \frac{\lambda_{dr}^s\omega_r^*}{\lambda_r^s} + \frac{\lambda_{dr}^s\lambda_s^*}{\lambda_r^s}\right\} - \frac{L_m n_p\omega_r\lambda_{qr}^s}{L_r} \quad (9)$$

where τ_r denotes the rotor time constant, ω_r^* is the reference rotor speed, λ_s^* is the reference stator flux linkage, and σ is the inductance factor of ASM as follows

$$\sigma = \frac{L_s L_r - L_m^2}{L_r} \quad (10)$$

2.3. Vectorized V/f (VV/Hz) Control

The standard open-loop V/f control approach is one of the simplest scalar drivers of the ASM because there is no need for the information of motor parameters and no necessity for close-loop regulation. To smoothly operate the motor at a desired switching frequency and with appropriate voltage vectors, a VV/Hz control baseline is developed in this work. The block diagram of the VV/Hz is illustrated in Fig. 4. The unique aspect of this controller is the fact that there is no inherent feedback and it is an open-loop controller. However, the block diagram shows that the motor speed is given feedback to generate voltage vectors for effective switching of VSI switches, although this is not necessary. The major advantage of using VV/Hz control is its simple structure to the DTC and IFOC as well as lesser parameter sensitivity. On the other hand, it has not been recognized as a high-performance approach for ASM drives due to its simple dynamic model.

According to Fig. 4, to produce the voltage vectors in the d-q axis, a PID speed controller is used to generate a d-axis command current along with the stator resistance R_s.

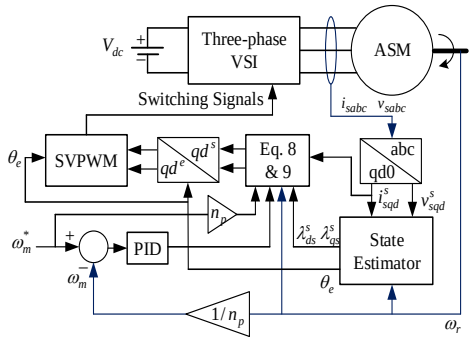

Fig. 3. Improved IFOC-SVPWM controlled ASM drive system.

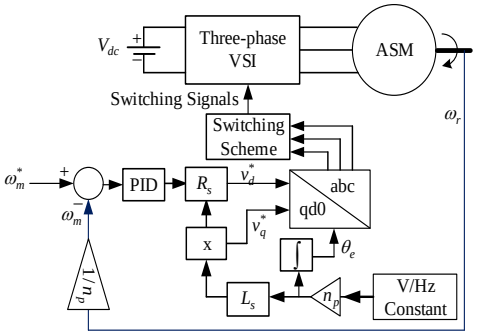

Fig. 4. VV/Hz controlled ASM drive system.

2.4. Feedback (FB) Linearization Control

Unlike the VV/Hz control, FB linearization baseline uses the feedback of several variables in its control algorithm [18]. According to Fig. 5, the feed backed variables are: stator currents, stator voltages, and rotor speed. The rotor flux is estimated from these variables. Rotor flux in the d-q axis along with its squared and derivate states, stator currents in the d-q axis, and squared rotor speed are delivered to the flux and speed controllers. The desired voltage signals are converted from the flux and speed controllers to the selected switching scheme. Consequently, the switching scheme produces gate pulses that will control the three-phase VSI-fed ASM.

The FB linearization approach, as a type of nonlinear mode feedback control, is completely separate input-output even in transient states. This control is different

from IFOC because IFOC is decoupled only when flux and speed are constant. The FB linearization control theoretically performs better than the IFOC because it takes into account the stator resistance voltage drops and other terms, allowing it to achieve perfect decoupling. The main disadvantage of this type of control is its additional parameter sensitivity, which results in a more complicated drive system.

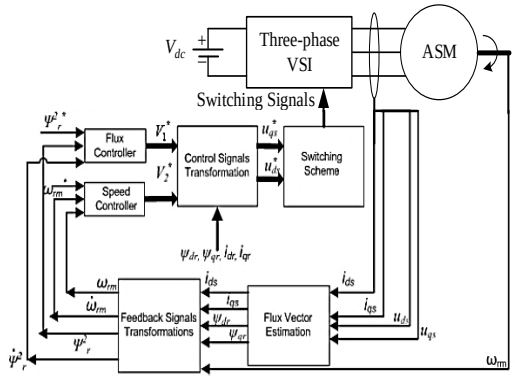

Fig. 5.ASM drive system with FB linearization.

Table 1. Nominal Parameters of the ASM Drive System

Parameter	Description	Value
P_m	Output power	3 hp
T_L	Rated torque	12 N.m
R_s	Stator resistance	1.5293 Ω
R_r	Rotor resistance	0.7309 Ω
L_s	Stator inductance	201.4 mH
L_r	Rotor inductance	203.1 mH
L_m	Magnetizing inductance	197.8 mH
n_p	Number of pole pairs	2
J_m	Rotor inertia	0.01 kg.m^2
B_m	Viscous friction coefficient	0.001 N.m.s/rad
V_{dc}	VSI DC link voltage	300 V

In the block diagram (Fig. 4), by measuring the three-phase currents and the motor speed and using the relations running the motor, the electromagnetic torque and the rotor flux as well as the position of the rotor flux angles are calculated. The calculated values of torque and rotor flux are added to the corresponding reference values and passing through a PI controller to produce the required reference stator currents. Using the abc to dq block whose inputs are the three-phase currents i_{abc} and the angle of position of the rotor flux, the actual currents i_{dq} are calculated and entered into the current control block with the corresponding reference values of i^*_{dq}. The outputs of this block generate V_{dq} voltages, which are converted to three-phase V_{abc} voltages to enter the gate signal generator. In this way, the input pulses of a three-phase inverter are obtained to generate and apply appropriate voltages to the stator terminals.

3. Comparative Studies and Results

The dynamic performances of the proposed control strategies are evaluated by MATLAB/Simulink R2023a functions for all the baselines and elements. To enable the switches of VSI, fixed switching frequency of 10 kHz at a sampling time of 5 μs is applied for all the simulations. The ASM drive system rated parameters that are used for simulations are listed in Table 1. Several case studies are implemented in dynamic modes and corresponding results are compared to validate the ASM drives' performance during different operational conditions.

3.1. Case 1: Step Change in the ASM Load Torque

The first test applies a step-down change from 4 to 3 N.m to the ASM load torque which is useful for determining which drive system has a better dynamic torque response. Considering the automobile industries, one application of this test can be the absolute acceleration control of a hybrid or electric vehicle from a stop or when entering the highways.

Fig. 6 shows the dynamic performance for the torque and speed of the ASM which is controlled by the conventional DTC and IFOC both equipped with the hysteresis regulators for the stator flux and torque based on band half width of 0.01, VV/Hz control, and FB linearization control. According to Fig. 6(a), the conventional DTC and FB linearization control have almost the same performance. However, the conventional IFOC and VV/Hz control include low-performance operations. As discussed earlier, both implemented conventional IFOC and DTC contain more torque ripples due to using the PWM switching techniques based on hysteresis current regulators. The dynamic responses of ASM speed during step-change of torque load are shown in Fig. 6(b). It is clear that the conventional DTC and FB linearization control strategies have better performances.

3.2. Case 2: Step Change in the ASM Motor Speed

The ASM is subjected to a step-down change in speed during this test from 100 to 80 rad/sec with a fixed load torque of 4 N.m. Fig. 7 shows the ASM torque and speed responses under the step change in speed. It is observed in Fig. 7(a) that the conventional DTC and IFOC baselines as well as FB linearization control have the closest responses, however, the VV/Hz control provides low performance with a slow transient state response. The steady-state error is around ± 1 percent of the rated speed. Considering the speed response illustrates the DTC-PWM baseline has the best performance, however, its torque response as depicted in Fig. 7(b), includes huge value variations during speed change than the other baselines. To encapsulate the ASM performance during this test, the DTC-PWM has an acceptable response for the speed control, and two other baselines including IFOC-PWM and FB linearization contain desired dynamic speed and torque responses.

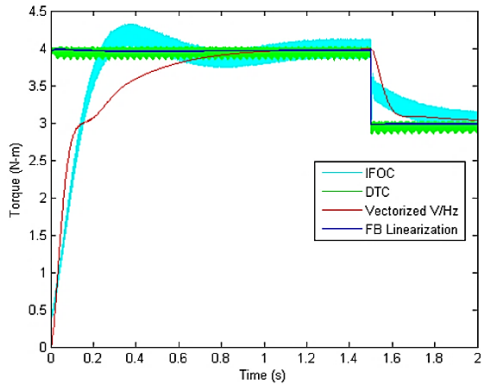

(a)

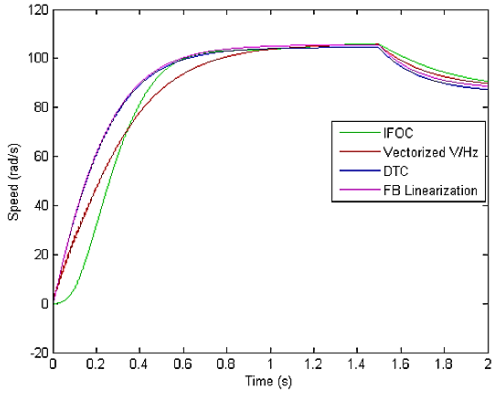

(b)

Fig. 6. Dynamic responses of the ASM during load change for, a) torque; b) speed.

3.3. Case 3: Dynamic Performance of the Improved Drives

As shown with earlier tests, two conventional baselines of DTC and IFOC with the PWM switching technique using hysteresis flux and torque regulators include low performance with more torque ripples leading to higher acoustic noises. Regarding the aforementioned solution for these issues, here, improved DTC and IFOC strategies with the SVPWM scheme are implemented to evaluate the impact of the PID regulators with the fixed switching frequency on the ASM drive system.

Fig. 8 shows the dynamic performance of the improved vector controlled ASM drive under the variable speed and torque loads. It is clearly illustrated in Fig. 8(a) that there are no remarkable ripples in the motor torque responses in comparison to their conventional versions with the PWM scheme leading to the smooth operation of the motor. From Fig. 8(b), the settling time of the improved control strategies is significantly reduced. By considering the SVPWM switching technique for the DTC and IFOC approaches, in identical test conditions, it seems that the IFOC baseline can be the best choice for the ASM drives in industries. However, if precise torque control is demanded, the DTC is a more feasible baseline than the other three approaches.

To practically compare the dynamic performance of the ASM drive under the aforementioned control strategies, two main operational criteria are chosen for speed including steady-state (S.S.) error after 2 s of running and settling (St.) time as listed in Table 2. These values are obtained under the command speed of 100 rad/s over a constant load torque. Based on Table 2, the FB linearization, IFOC-PWM, and DTC-PWM approaches have similar performance, while the VV/Hz approach includes a weaker performance. Moreover, the DTC is the fastest motor controller that can drive the ASM to 100 rad/s in 0.1 s. It is clear from Table 2 that the IFOC has a very similar performance with DTC by a time of 0.102 s to reach steady-state operation.

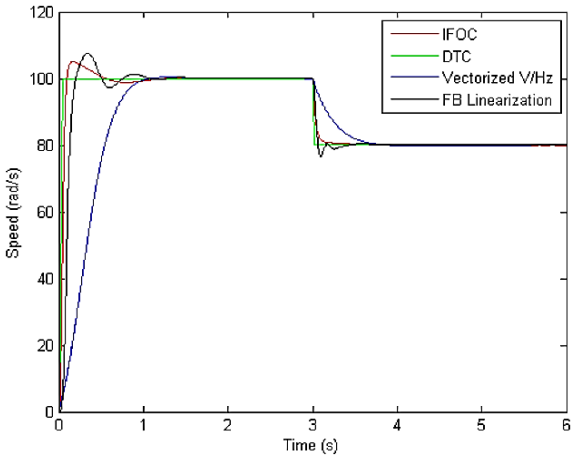

(a)

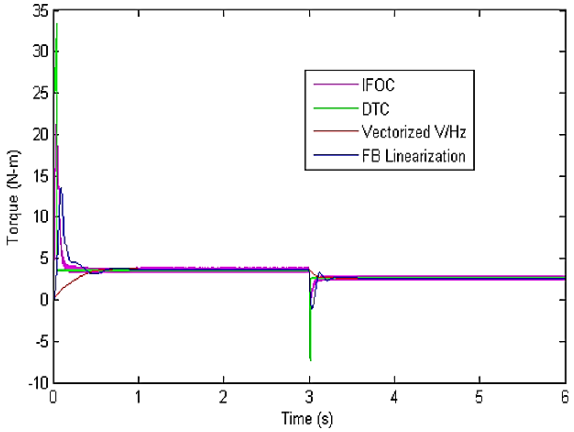

(b)

Fig. 7. Dynamic responses of the ASM during speed change for, a) speed; b) torque.

Table 2. Performance Comparison of the ASM Drive

Baseline / Criterion	IFOC	DTC	FB Linearization	VV/Hz
S.S. Error (%)	0.28	0.29	0.20	0.41
St. Time (s)	0.102	0.100	0.270	0.545

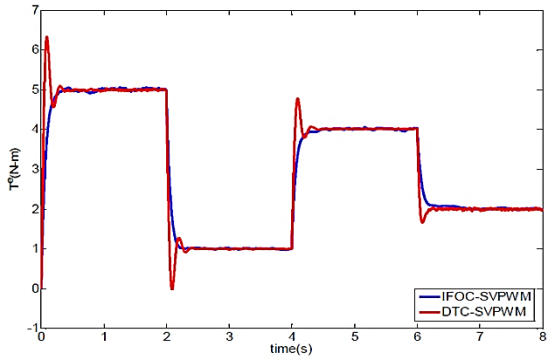

(a)

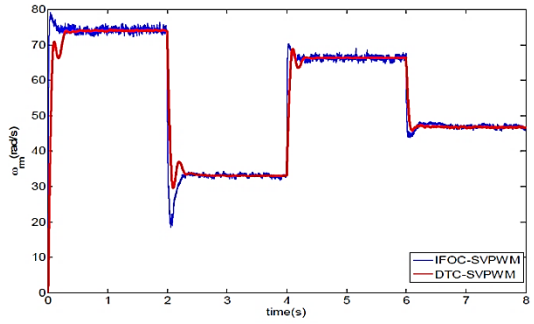

(b)

Fig. 8. Dynamic responses of the improved vector-controlled ASM, a) torque; b) speed.

4. Conclosions

This paper concentrated on the development of improved vector and scalar control strategies for three-phase ASM drive dynamic behavior assessment using MATLAB/Simulink functions. The computer-aided simulations were performed on the three-phase VSI-fed ASM to demonstrate the overall performance of the four aforementioned control approaches. The simulation results showed that DTC and FB linearization control strategies have the best torque dynamic performance. On the other hand, The IFOC has comparable torque performance when SVPWM is used as the switching scheme instead of standard current hysteresis regulators with the PWM technique. Based on the speed test, it is clarified that the FB linearization, DTC, and IFOC perform similarly, while the vectorized V/f control includes poor responses. Furthermore, the robustness of the developed DTC-SVPWM and IFOC-SVPWM strategies have been evaluated over variable speeds and load torque profiles.

References

[1] S. P. Biswas, M. S. Anower, S. Haq, M. R. Islam, M. A. Rahman, and K. M. Muttaqi, “A New Level Shifted Carrier-Based PWM Technique for a Cascaded Multilevel Inverter Based Induction Motor Drive,” in *IEEE Transactions on Industry Applications*, vol. 59, no. 5, pp. 5659-5671, Sept.-Oct. 2023.

[2] M. Ebadpour, M.B.B. Sharifian, “Cascade H-Bridge Multilevel Inverter with Low Output Harmonics for Electric/Hybrid Electric Vehicle Applications,” *International Review of Electrical Engineering (IREE)*, vol. 7, no. 1, pp. 3248-3256, February 2012.

[3] V. F. Pires, A. Cordeiro, D. Foito, J. F. Silva and E. Romero-Cadaval, “Cascaded Multilevel Structure With Three-Phase and Single-Phase H-Bridges for Open-End Winding Induction Motor Drive,” in *IEEE Open Journal of the Industrial Electronics Society*, vol. 4, pp. 346-361, 2023.

[4] Z. Tir, T. Orlowska-Kowalska, H. Ahmed and A. Houari, “Adaptive High Gain Observer Based MRAS for Sensorless Induction Motor Drives,” in *IEEE Transactions on Industrial Electronics*, vol. 71, no. 1, pp. 271-281, Jan. 2024.

[5] M. Ebadpour, M. Jamshidi, J. Talla, H. Hashemi-Dezaki, Z. Peroutka, “Digital Twin Model of Electric Drives Empowered by EKF,” *Sensors*, vol. 23, no. 4, pp. 1-21, Feb. 2023.

[6] M. Nagataki, K. Kondo, O. Yamazaki and K. Yuki, “First-Order-Delay-Controlled Slip-Angular Frequency for the Dynamic Performance of an Indirect-Field-Orientation-Controlled Induction Motor-Driving Inertial Load,” in *IEEE Open Journal of Industry Applications*, vol. 4, pp. 160-177, 2023

[7] B. Çavuş and M. Aktaş, “MPC-Based Flux Weakening Control for Induction Motor Drive With DTC for Electric Vehicles,” in *IEEE Transactions on Power Electronics*, vol. 38, no. 4, pp. 4430-4439, April 2023.

[8] G. Singh, K. Nam, and S. K. Lim, "A simple indirect field-oriented control scheme for multiphase induction machine," *IEEE Trans. Ind. Electron.*, vol. 52, no. 4, pp. 1177–1184, Aug. 2005.

[9] W. Tian *et al*., "Fast Indirect Model Predictive Control for Variable Speed Drives," in *IEEE Transactions on Power Electronics*, vol. 38, no. 11, pp. 14475-14491, Nov. 2023.

[10] S. Kim, I. Yoon, C. Hong, J. Ko and S. Oh, "A study on a new sensorless control method for an induction motor using a non-linear speed observer and hybrid V/f control method," *2023 IEEE Texas Power and Energy Conference (TPEC)*, College Station, TX, USA, 2023, pp. 1-5.

[11] K. B. Hunasikatti, R. L. Naik and B. V. Hiremath, "Implementation of FPGA Based Closed Loop V/f Speed Control of Induction Motor Employed for Industrial Applications," *2018 Second International Conference on Advances in Electronics, Computers and Communications (ICAECC)*, Bangalore, India, 2018, pp. 1-6.

[12] H. Swami and A. Kumar Jain, "An Improved Vector Controlled Induction Motor Drive Using Proportional Integral Type of Current Controllers in Stationary Reference Frame," *IECON 2023- 49th Annual Conference of the IEEE Industrial Electronics Society*, Singapore, Singapore, 2023, pp. 1-8.

[13] M.B.B. Sharifian, B. Yousefi, M. Ebadpour, "A New Hybrid Anti-Lock Braking System for HEVs Based on Optimal Slip Control Using DTFC," *Journal of Science International-Lahore*, vol. 1, no. 26, pp. 197-203, 2014.

[14] H. Sudheer, S. K. Fodad and B. Sarvesh, "Implementation of SVM-DTC of induction motor using FPGA," *2017 IEEE International Conference on Power, Control, Signals and Instrumentation Engineering (ICPCSI)*, Chennai, India, 2017, pp. 2319-2323.

[15] R. Kumar, P. Kant, and B. Singh, "An 18-pulse converter and 4-level cascaded inverter based induction motor drive," *IEEE Trans. Ind. Appl.*, vol. 58, no. 3, pp. 4122–4133, May/Jun. 2022.

[16] A.Sudaryanto *et al*., "Design and Implementation of SVPWM Inverter to Reduce Total Harmonic Distortion (THD) on Three Phase Induction Motor Speed Regulation Using Constant V/F," *2020 3rd International Seminar on Research of Information Technology and Intelligent Systems (ISRITI)*, Yogyakarta, Indonesia, 2020, pp. 412-417.

[17] E.H.E. Bayoumi, "Multi-resolution analysis wavelet PI stator resistance estimator for direct torque induction motor drive", *WSEAS Trans. Circuits and Systems*, vol. 12, no. 7, pp.211–220, 2013.

[18] Z. Krzeminski, "Nonlinear controllers for induction motors", in Proceedings of the 10th IFAC World Congress, Munich, 1987, pp. 349-354.